

## PERFORMANCE STUDIES OF MINIATURIZED CYLINDRICAL AND ANNULAR HALL THRUSTERS

A. Smirnov, Y. Raitses, and N. J. Fisch

Princeton University Plasma Physics Laboratory, Princeton, NJ

### Abstract

Conventional annular Hall thrusters do not scale efficiently to low power. An alternative approach, a 2.6 cm miniaturized cylindrical Hall thruster with a cusp-type magnetic field distribution, was developed and studied. Its performance was compared to that of a conventional annular thruster of the same dimensions. The cylindrical thruster exhibits discharge characteristics similar to those of the annular thruster but has much higher propellant ionization efficiency. Significantly, a large fraction of multicharged xenon ions might be present in the outgoing ion flux generated by the cylindrical thruster. The operation of the cylindrical thruster is quieter than that of the annular thruster. The characteristic peak in the discharge current fluctuation spectrum at 50-60 kHz appears to be due to ionization instabilities. In the power range 50-300 W, the cylindrical and annular thrusters have comparable efficiencies ( $\eta=15-32\%$ ) and thrusts ( $T=2.5-12$  mN). For the annular configuration, the voltage less than 200 V was not sufficient to sustain the discharge at low propellant flow rates. The cylindrical thruster can operate at voltages lower than 200V, which suggests that a cylindrical thruster might be designed to operate at even smaller power.

### Introduction

There is a strong interest in low-power propulsion devices within the space community. This interest is driven by the desire to reduce the spacecraft mass. A decrease in a spacecraft mass can significantly reduce launch cost and, therefore, enable new scientific and exploration space missions, which involve multiple microspacecraft flying in constellations.<sup>1,2</sup> The Hall thruster<sup>3</sup>, as a mature electric propulsion device, seems very promising for low-power primary propulsion on near-Earth missions<sup>4</sup> (orbit transfer, repositioning, etc.).

Scaling down the operating power of a Hall thruster requires reducing the discharge voltage or the discharge current. The degree to which the first option can be accommodated is limited by the desire to keep

the exhaust ion velocity high. The second option implies that the propellant flow rate should be decreased. In order to maintain high propellant utilization efficiency at low propellant flow rates, the thruster channel must be scaled down to preserve the ionization probability. Then, according to Ref. (5), the length of the acceleration region, which is mainly determined by the magnetic field distribution, must decrease linearly with the channel sizes, while the magnetic field must increase inversely to the scaling factor. However, the implementation of the latter requirement is technically challenging because of magnetic saturation in the miniaturized inner parts of the magnetic core. A linear scaling down of the magnetic circuit leaves almost no room for the use of thin magnetic poles or for heat shields, making difficult the achievement of the optimal magnetic fields. Nonoptimal magnetic fields result in enhanced power and ion losses, heating and erosion of the thruster parts, particularly the critical inner parts of the coaxial channel and magnetic circuit.

Currently existing low-power Hall thruster laboratory prototypes with channel diameters 2-4 cm operate at 100-300 W power levels with efficiencies in the 10-40% range.<sup>6-8</sup> However, further scaling of a Hall thruster of the conventional geometry down to sub-centimeter size<sup>9</sup> resulted in even lower efficiencies (6% at about 100 W). The low efficiency might arise from a large axial electron current, enhanced either by magnetic field degradation due to excessive heating of the thruster magnets or by electron collisions with the channel walls. These results make the usefulness of simply miniaturizing the conventional annular Hall thruster debatable.

The cylindrical Hall thruster suggested in Ref. (10) features a channel with a short annular region and longer cylindrical region, and a cusp-type magnetic field distribution (see Fig. 1a). Having larger volume to surface ratio than the conventional annular thruster, and therefore, potentially smaller wall losses in the channel, the cylindrical Hall thruster should suffer lower erosion and heating of the thruster parts. This makes the concept of a cylindrical Hall thruster very promising for low-power applications.

A relatively large 9 cm diameter version of the cylindrical thruster exhibited performance comparable with conventional annular Hall thrusters in the sub-kilowatt power range<sup>10</sup>. In the present work we developed and studied a miniaturized 2.6 cm diameter cylindrical Hall thruster. In order to better understand the physics of cylindrical Hall thrusters and to examine the attractiveness of the cylindrical approach for low-power Hall thruster scaling, we compared the performance of 2.6 cm cylindrical Hall thruster to that of the conventional annular thruster with the same channel diameter and length. Thruster ac and dc electrical measurements, as well as total ion flux and thrust measurements were performed. It was found that the cylindrical thruster has unusually high propellant ionization efficiency, compared to conventional Hall thrusters. The ratio of the total ion current to the effective propellant mass flow current, in the case of cylindrical configuration, could exceed 1, which clearly indicates the presence of multicharged Xe ions in the ion flux generated by the thruster. The discharge in the cylindrical thruster was also found to be somewhat quieter than that in the annular thruster: The amplitude of oscillations in the frequency range 10 - 100 kHz was relatively lower for the cylindrical configuration. However, the spectrum of discharge current oscillations of the cylindrical thruster exhibits a pronounced peak at about 50-60 kHz, which may be due to ionization instabilities.<sup>11</sup> The effects of higher ionization efficiency and quieter operation of the cylindrical thruster are very interesting and the underlying physics deserves further study.

### Experimental Setup

A 2.6 cm cylindrical Hall thruster shown in Fig. 1 was scaled down from a 9 cm cylindrical Hall thruster to operate at ~ 200 W power level.<sup>12</sup> Similar to the large thruster, this miniaturized cylindrical thruster consists of a Boron Nitride ceramic channel, an annular anode, which is also a gas distributor, two electromagnetic coils, and a magnetic core. Field lines of the cusp-type magnetic field intersect the ceramic channel walls. The electron drift trajectories are closed. Magnetic field lines form equipotential surfaces, with  $E = -v_e \times B$ . Ion thrust is generated by the axial component of the Lorentz force, which is proportional to the radial magnetic field and azimuthal electron current.

The cylindrical channel features a short annular region, approximately 1 cm long, and longer cylindrical region. The total length of the channel is 2.6 cm. The length of the annular region was selected so as to provide high ionization of the working gas at the boundary of annular and cylindrical regions. The outer and inner diameters of the channel are 2.6 cm and 1.4 cm, respectively. The thruster design allows one to vary

the thruster geometry. By extending the central pole of the magnetic core and the central ceramic piece up to the exit plane of the channel, the cylindrical thruster can be converted to the conventional annular one. In this study we investigated two thruster configurations, namely, cylindrical with the dimensions specified above, and annular with the same channel OD, ID, and length. The overall diameter and length of the thruster were both 7 cm.

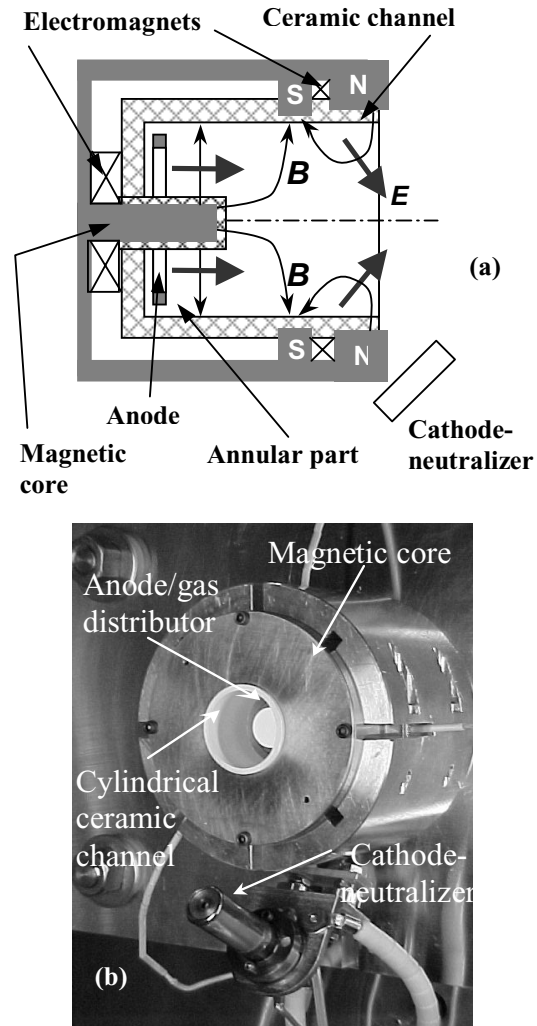


Fig. 1. a) Schematic of a cylindrical Hall thruster. b) The 2.6 cm cylindrical Hall thruster.

Two electromagnetic coils were connected to separate power supplies. The currents in the coils were co-directed in conventional configuration and counter-directed in cylindrical configuration to produce cusp magnetic field with a strong radial component in the channel. Fig. 2 shows simulated results of the magnetic field distribution for the annular and cylindrical thrusters. The magnetic field was measured inside both

these thrusters with a miniature Hall probe with dimensions 1.5 mm x 1.5mm. The results of these measurements and simulations are in a good agreement.

For example, for the operating currents of 1.4 A in the back coil and 0.9 A in the front coil, the maximum radial magnetic field is 400 G at the inner wall near the exit of the annular channel. In the cylindrical configuration, the radial magnetic field reaches the maximum,  $\sim 700$  G, a few millimeters from the anode near the inner wall of the short annular part and then reduces towards the thruster exit.

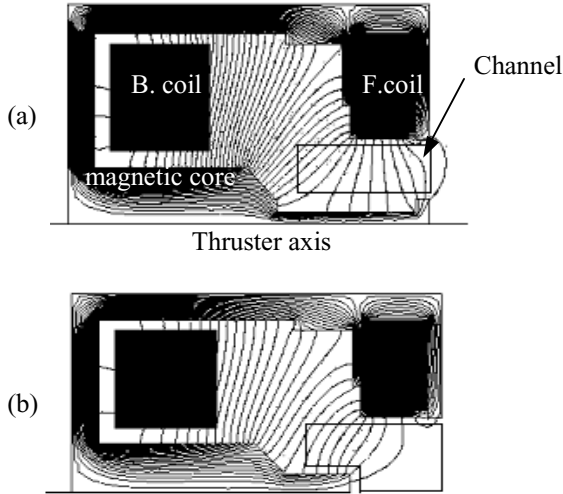


Fig. 2. Magnetic circuit and the magnetic field distribution for the annular (a) and cylindrical (b) thrusters. The channel outer diameter is 2.6 cm.

The experiments took place in a  $0.4\text{-m}^3$  vacuum chamber, equipped with a turbo molecular pumping system (PPPL Small Hall Thruster facility). The measured pumping speed reached  $\sim 1700 \pm 300$  l/s for xenon. The working background pressure of Xe was about  $7 \times 10^{-5}$  Torr for the total propellant flow rate of 0.8 mg/s. Uncertainty in the determination of the pumping speed was caused by discrepancies in the readings of two Bayard-Alpert tabulated ion gauges used to measure the background pressure. Two commercial flow controllers, 0-10 sccm and 0-15 sccm, volumetrically calibrated in the flow rate range of 1-10 sccm, supplied research grade xenon gas to the anode and the cathode, respectively. A commercial HeatWave plasma source was used as a cathode-neutralizer. The cathode flow rate of xenon was held at 0.2 mg/s for all the experiments.

The total ion flux coming from the thruster and the plume angle were measured by a movable electrostatic graphite probe with a guarding sleeve. Graphite was chosen as a probe material because it has an extremely low sputtering coefficient for Xe ions with

energies lower than or about 500 eV. The probe can be rotated in the vertical plane  $\pm 90$  deg relative to the thruster exit. The collecting surface of the probe always points at the center of the thruster. The distance between the probe and the thruster center is 14 cm. Yet another probe mounted on the same movable arm was used to measure the flux of backstreaming ions. The second probe is horizontally shifted about 2 cm away from the first one, and its collecting surface points out from the thruster.

Measurements of the thrust were performed in the Electric Propulsion and Plasma Dynamics Laboratory (EPPDL) at Princeton University. The EPPDL thrust stand<sup>13</sup> was designed to measure accurately impulse bits for pulsed plasma thrusters (PPTs) within the range of  $10^{-4} - 10$  Ns. However, it was also theoretically predicted to be capable of measuring low steady state thrust, as low as  $20 \mu\text{N}$ .

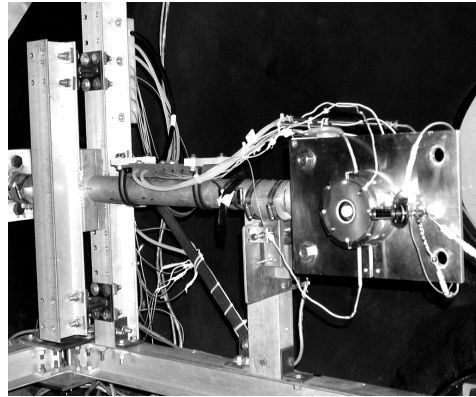


Fig. 3. 2.6 cm annular Hall thruster mounted on the thrust stand.

The thruster was mounted on a swinging arm thrust stand.<sup>14</sup> Fig. 3 shows a 2.6 cm annular Hall thruster attached to the arm. The thrust arm is mounted with two flexural pivots. Thrust arm displacement from the equilibrium position is measured by a linear voltage differential transformer.

During steady-state thruster operation, the thrust generated by the thruster is directly proportional to the displacement of the thrust arm:

$$T = k_{eff}(x - x_{equil}), \quad (1)$$

where  $k_{eff}$  is the effective spring constant of the thrust stand. The effective spring constant is due to torsion exerted in the pivots, as well as restoring forces produced by the thruster wiring and the flexible silicon gas line (see Fig. 3), which connect the thruster with a fixed rigid part of the stand. In the present setup, it is impossible to eliminate the contribution of the wiring and the gas line to the effective spring constant.

Although experimentally minimized, this contribution was on the order of the torsional spring constant of the flexural pivots.

It should be mentioned that for the same discharge voltage, coil currents, and propellant flows values of the discharge current measured at the EPPDL vacuum facility<sup>13</sup> were generally about 10% lower than those measured at the PPPL Small Hall Thruster facility. This apparently was due to the fact that the operating background pressure of Xe (about  $1 \times 10^{-5}$  Torr for the total propellant flow rate of 0.8 mg/s) was typically 5-7 times lower than that at the PPPL facility.

### Experimental Results and Discussion

#### Ion current and V-I characteristics

The 2.6 cm Hall thruster was operated at the discharge voltages of 150 - 300 V and xenon mass flow rates of 0.4 – 0.8 mg/s. The cathode was placed near the thruster exit at the 30 degrees angle to the thruster axis (See Fig. 1). The operation of the thruster in the cylindrical and annular configurations is shown in Fig. 4.

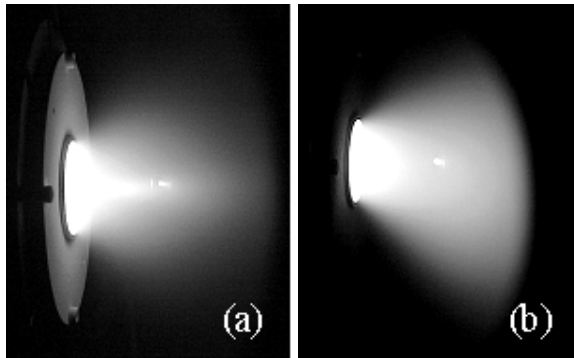


Fig. 4. Thruster operation in the annular (a) and cylindrical (b) configurations.

Illustrative curves of voltage versus current characteristics measured for each thruster configuration are shown in Fig. 5a. At given discharge voltage and propellant flow rate, the discharge current, and, consequently, also the input power in the cylindrical thruster, are both larger than those in the annular thruster by factor of 1.5-2. However, the current utilization efficiency, which is the ratio of the ion current at the exit plane of the thruster to the total discharge current, differs on average by about 10% only at voltages of 250-300 V (See Fig. 5b). The reason for this is an exceptionally high propellant ionization efficiency of the cylindrical thruster.

The ionization efficiency of a thruster is characterized by a so-called propellant utilization

coefficient  $\eta_I$  – a ratio of the total ion current  $I_i$  at the exit plane of a thruster to the propellant flow rate  $\mu$  expressed in units of electric current.  $\eta_I = I_i M / e \mu$ , where  $M$  is a mass of a propellant atom,  $e$  is the electron charge. In Fig. 6  $\eta_I$  is plotted vs. discharge voltage for the cylindrical and annular configurations. Propellant utilization for the cylindrical configuration can be seen to be much higher than that for the annular one. It increases with the discharge voltage and exceeds 1 at high voltages, which implies a presence of xenon ions in charge states higher than +1 in the ion flux.

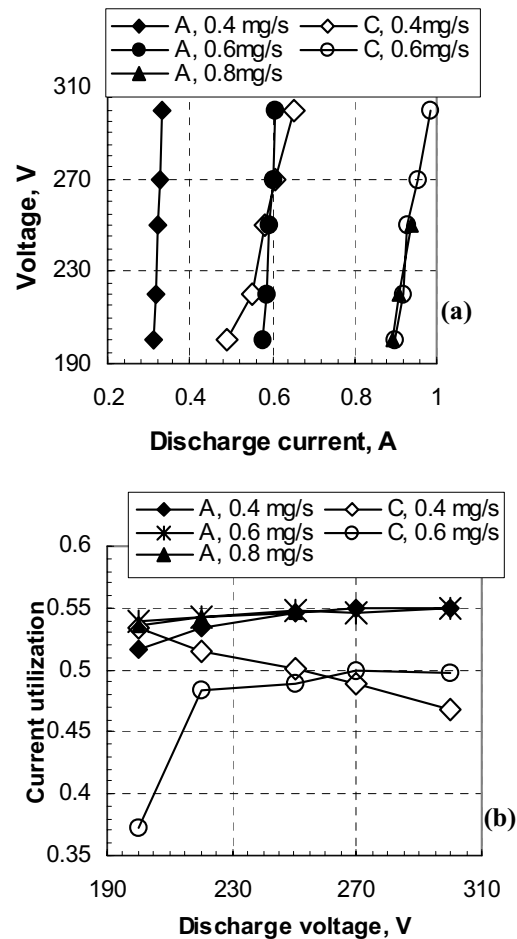


Fig. 5. a) Discharge voltage versus current characteristics for the 2.6 cm cylindrical (C) and annular (A) thrusters (as measured at the PPPL experimental facility). The cathode flow rate is 0.2 mg/s. b) Ratio of the ion current at the exit of the thruster to the discharge current versus discharge voltage.

The increase in propellant utilization in the cylindrical configuration might be explained by ionization enhancement due to an increase in the

electron density. As seen from Fig 5b, the electron current to the anode in the cylindrical thruster is larger than in the annular. On the other hand, the electron mobility across the magnetic field should be lower in the cylindrical configuration, because the radial component of the magnetic field is typically 1.5-2 times larger than that in the annular. Therefore, the electron density in the channel is expected to be higher in the cylindrical configuration. Simple estimates show that a 25% increase in the propellant utilization (see Fig. 6) requires only about a twofold increase in the electron density. However, an increase in the radial magnetic field in a conventional annular thruster does not lead to a corresponding increase in the electron density, because of the onset of strong high-frequency discharge current oscillations.<sup>11</sup>

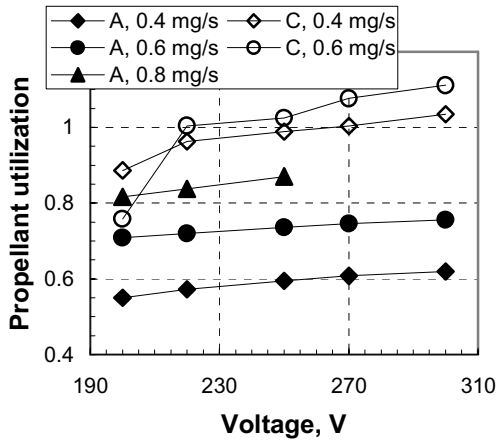


Fig. 6. Propellant utilization coefficient versus discharge voltage for the 2.6 cm cylindrical (C) and annular (A) thrusters

The fact that the ion flux produced by the thruster can contain a substantial portion of multiply charged Xe ions is of particular interest. It is worth mentioning that even in conventional Hall thrusters, where the propellant utilization coefficient is typically 0.8-0.9, an ion flux can have rather large fractions of  $Xe^{2+}$  and  $Xe^{3+}$  ions.<sup>15</sup> The major factor in multicharged ions formation in a Hall thruster is the ion residence time in the channel. Simple estimates show that the time of flight of a  $Xe^+$  ion through a channel is much smaller than the time of ionization to higher charge states. Indeed, one expects a plasma in a miniaturized Hall thruster to have electron density of about  $10^{12} \text{ cm}^{-3}$  and electron temperature of 10-20 eV.<sup>16</sup> For example, for  $T_e \sim 20$  eV the rate coefficient for single electron impact ionization  $Xe^{+1} \rightarrow Xe^{+2}$  is about  $k_{1,2} \sim 4 \times 10^{-8} \text{ cm}^3/\text{s}$ .<sup>17</sup> Therefore, even for a moderately energetic ion with  $E_i=50$  eV, the time of flight through a channel with

length  $L = 3 \text{ cm}$   $\tau_f \sim L/V_f \sim 4 \times 10^{-6} \text{ s}$  is approximately an order of magnitude smaller than the ionization time  $\tau_{1,2} \sim (n_e k_{1,2})^{-1} \sim 3 \times 10^{-5} \text{ s}$ . Thus, in this regime, we expect that the number of ionization events should scale linearly with the residue time. The presence of a significant number of multicharged ions in the outgoing ion flux might be an indication of a complex ion dynamics (possibly, non-straight trajectories, trapping by ambipolar potential, etc.) which increases the ion life time in the channel. Formation of an ion charge state distribution in a Hall thruster discharge deserves further study.

### Discharge Oscillations

Typical spectra of the discharge current oscillations are shown in Fig. 7. Although the amplitude of oscillations is relatively lower for the cylindrical configuration, the discharge at low propellant flow rates is not as quiet as it was found to be in the large 9 cm cylindrical thruster.<sup>10</sup> The characteristic peak at frequencies  $\sim 50$ -60 kHz may be due to an ionization instability, which appears because of the depletion of neutral atoms in the ionization and acceleration regions.<sup>11</sup> The characteristic frequency of these oscillations scales as  $f \sim v_n/L_i$ , where  $v_n$  is the thermal speed of a neutral atom and  $L_i$  is a length of the ionization region. Apparently, the characteristic frequency, which was typically  $\sim 20$  kHz for a 9 cm annular Hall thruster,<sup>10</sup> almost triples as  $L_i$  together with the thruster sizes are reduced by about factor of 3.

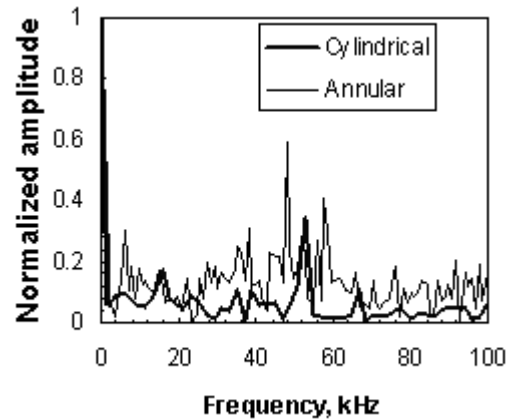


Fig. 7. Spectra of discharge current oscillations for the annular and cylindrical thrusters at  $U_d=300 \text{ V}$  and anode flow rate of  $0.4 \text{ mg/s}$ .

### Thrust and Efficiency

As mentioned above, the thrust stand had not been specifically designed to suit the experimental environment of a steady state Hall thruster operation.

Thruster operation showed that the heat generated by the thruster brought about a weak long-timescale thermal drift of the thrust stand equilibrium position. The larger the thruster operating power was, the more visible this effect became. However, it was experimentally found that the thrust stand moment of inertia remained almost unaffected by a temperature change due to the thruster operation.

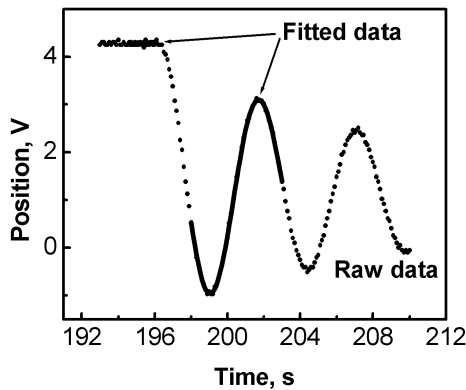


Fig. 8. An exemplary trace of thrust arm position vs. time. At  $t \approx 196.3$  s the thruster was turned off. Time interval from 198 s to 203 s is used for curve fitting with a damped linear oscillator response function (solid line) to determine the instantaneous equilibrium position. A 2-sec interval (solid line) before the turning off is used to determine the displacement of the arm caused by the produced thrust.

In order to minimize the uncertainty of the thrust measurements caused by the equilibrium position drift, a procedure to determine an ‘instantaneous’ equilibrium position and  $k_{eff}$ , was developed. Once the steady state operation of the thruster was achieved (about 20 min. from the ignition of the discharge), the discharge voltage, coil power, and gas flow to the anode and cathode were turned off, and oscillations of the thrust arm position  $x(t)$  were recorded (see Fig. 8).

The position of the thrust arm  $x_0$  corresponding to the firing thruster was determined from averaging  $x(t)$  over a 2-second interval immediately before the turning off. The instantaneous equilibrium position  $x_{equil}$  together with  $k_{eff}$  was determined from fitting approximately half of the period of oscillations right after the turning off with a damped linear oscillator response function.<sup>13</sup> The thrust was calculated then according to Eq. (1). For each set of operating parameters the thrust measurement was repeated several times to minimize the statistical error. This measurement procedure ensured good repeatability of results.

Figure 9 shows measured thrust versus discharge voltage and efficiency versus input power for different anode flow rates for the cylindrical and annular configurations of 2.6 cm Hall thruster. In all regimes but one, the estimated error bars on thrust and efficiency are  $\pm 3\%$  and  $\pm 6\%$ , respectively, which is comparable with typical values of errors for most of the low-thrust measurements.<sup>6,7</sup> In the case of cylindrical configuration with anode flow rate of 0.7 mg/s the error bars are  $\pm 6\%$  for thrust and  $\pm 12\%$  for efficiency. These relatively larger measurement errors are due to the more pronounced thrust stand thermal drift, observed at high operating power, and, partly, to the unstable operation of the anode in this particular regime. Unstable operation of the anode was supposedly caused by the anode overheating.

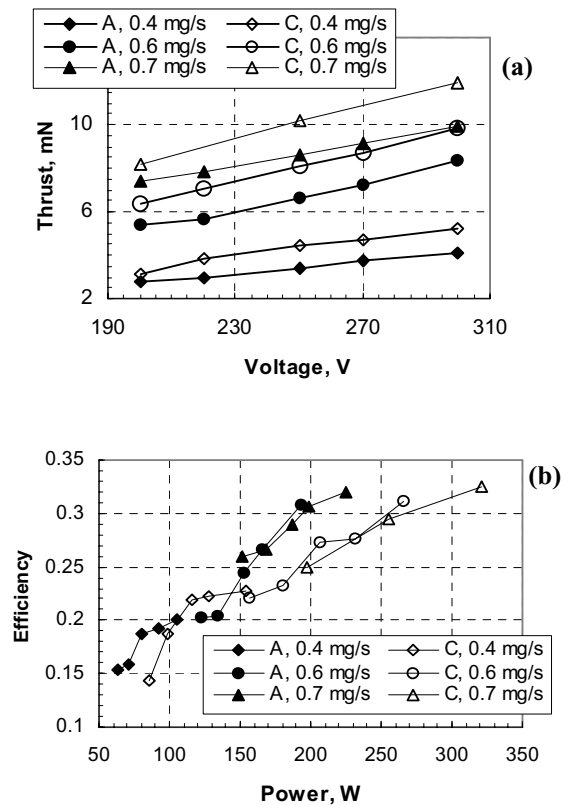


Fig. 9. a) Measured thrust vs. discharge voltage and b) efficiency as a function of input power for different anode flow rates for the 2.6 cm cylindrical (C) and annular (A) thrusters. The estimated error bars on thrust and efficiency are  $\pm 3\%$  and  $\pm 6\%$ , respectively, for all regimes except for the case of cylindrical configuration with anode flow rate of 0.7 mg/s, where the error bars are  $\pm 6\%$  for thrust and  $\pm 12\%$  for efficiency.

Measured thrust ranges from about 3 mN (200V, 86 W) to 12 mN (300V, 320W) for the cylindrical configuration, and from about 2.5 mN (200V, 63W) to 10 mN (300V, 225W) for the annular configuration. For any given discharge voltage and anode flow rate in the range of parameters investigated, the thrust generated in the cylindrical configuration is larger than that in the annular configuration. This is another indication that the cylindrical configuration has a better propellant ionization capability (see Fig. 6).

It should be mentioned that the cylindrical thruster can be operated at the discharge voltage lower than 200 V, while for the annular configuration such voltage is not sufficient to sustain the discharge at low propellant flow rates. In Fig. 9, the voltage is kept at least at 200 V only in order to make comparison between the two configurations.

The efficiency  $\eta$  was calculated, using the measured thrust  $T$ , flow rate  $\mu$  and power  $P$ , as  $\eta = T^2 / 2\mu P$ . The cathode power and propellant flow and the magnet losses were not taken into account. Therefore, the efficiency plotted in Fig. 9b is a so-called 'anode' efficiency. As can be seen from the graphs, the cylindrical and annular thrusters have comparable efficiencies. This, in principle, gives an opportunity to develop a low-power Hall thruster capable of generating a variable thrust at given efficiency and thruster power. The use of a variable-thrust thruster is required for optimization of a propellant expenditure on satellites.<sup>18</sup> Thrust variation can be achieved in the 2.6 cm Hall thruster by changing the length of the central magnetic pole and channel piece. At constant power, one can increase the thrust (and decrease the ion exhaust velocity) by converting the thruster from the cylindrical to the annular configuration. For example, at power of about 120 W (see Fig. 9a and 9b), the transition between  $\mu=0.4$  mg/s and  $U_d=250$  V in the cylindrical configuration and  $\mu=0.6$  mg/s and  $U_d=200$  V in the annular configuration decreases efficiency by less than 2%, while the increase in thrust is 21%.

### Conclusions

Annular conventional Hall thrusters do not scale efficiently to small sizes because of the large surface to volume ratio and the difficulty in miniaturizing the magnetic circuit. An alternative approach, which may be more suitable for scaling to low power, is a cylindrical Hall thruster. A 2.6 cm miniaturized cylindrical Hall thruster was developed and operated in a broad range of operating parameters. Its performance was compared to that of a conventional annular thruster of the same dimensions. Several interesting effects were observed.

The ion flux and thrust measurements showed that propellant ionization efficiency of the cylindrical thruster is much higher than that of the annular. Therefore, gases or gas mixtures that are harder to ionize than xenon may be used as a propellant; for example, one can use argon to generate larger ion exhaust velocities. In the cylindrical thruster, at high propellant flow rates, a significant fraction of multicharged xenon ions can be present in the outgoing ion flux. This may indicate complex ion dynamics that increase the ion life time in the channel. The formation of multicharged ions in a cylindrical Hall thruster discharge, which may be very different from that in an annular thruster, is a subject of ongoing research.

Discharge characteristics of the cylindrical thruster are comparable to those measured for the annular thruster. Although relatively quieter operation of the cylindrical thruster was observed, the discharge at low propellant flows is not as quiet as it was found to be in the large 9 cm cylindrical thruster. The characteristic peak at frequencies  $\sim 50$ -60 kHz may be due to an ionization instability, whose frequency approximately triples as the thruster sizes are reduced by a factor of 3.

At given discharge voltage and propellant flow rate, the discharge current and input power of the cylindrical thruster are higher than those of the annular one. The higher power and current would tend to erode the thruster faster; on the other hand, the cylindrical thruster has a lower surface to volume ratio and fewer inner parts. The lifetime comparison, therefore, remains an open question.

In the power range 50-300 W, the cylindrical and annular thrusters have comparable efficiencies ( $\eta=15$ -32%) and thrusts ( $T=2.5$ -12 mN). Since these configurations may be controlled electronically, it may be possible to develop an efficient low-power Hall thruster with a variable thrust.

The values of efficiency for both configurations are comparable to those of other currently existing Hall microthrusters. For example, BHT-200-X2B<sup>6</sup> has channel diameter  $d=2.1$  cm and operates at power  $P=100$ -300 W with efficiency  $\eta = 20$ -45%, SPT-30<sup>7</sup> has  $d=3$  cm,  $P=100$ -260 W, and  $\eta=16$ -34%.

For the annular configuration, a voltage less than 200 V was not sufficient to sustain the discharge at low propellant flow rates. However, the cylindrical thruster can operate at low voltages ( $U_d < 200$ V). Operation at low voltage is important for three reasons: one, certain missions may require lower ion exhaust velocity. Two, voltages lower than 200 V may be accommodated by direct drive power, which could simplify enormously the power processing unit on a small satellite. Three, the operation at low voltage suggests that further miniaturization may be possible, thereby permitting even lower power operation.

### Acknowledgments

The authors would like to thank Prof. Edgar Choueiri for the provided opportunity to work with the EPPDL thrust stand, Kurt Polzin for his assistance in the thrust measurements, and David Staack for the help in the experiments at the PPPL facility.

This work was supported by grants from AFOSR and DARPA.

### References

1. R.M. Jones, Journal of the British Interplanetary Society, **42**(10), 2588 (1989)
2. R.L. Ticker, D. McLennan, *Proceedings of IEEE Aerospace Conference*, Big Sky, MN, 2001
3. A.I. Morozov and V.V. Savelyev, in *Review of Plasma Physics*, edited by B.B. Kadomtsev and V.D. Shafranov (Consultants Bureau, New York, 2000), Vol. 21, p. 203.
4. J. Mueller, in *Micropropulsion for Small Spacecraft*, edited by M.M. Micci and A.D. Ketsdever (AIAA Progress in Astronautics and Aeronautics, 2000), Vol. 187, p. 45.
5. J. Ashkenazy, Y. Raitses, and G. Appelbaum, *Proceedings of the 2<sup>nd</sup> International Spacecraft Propulsion Conference*, Holland, 1997.
6. V. Hruby, J. Monheiser, B. Pote, C. Freeman, and W. Connolly, IEPC paper 99-092, 26<sup>th</sup> International Electric propulsion Conference, Kitakyushu, Japan, June 1999.
7. D. Jacobson and R. Jankovsky, AIAA paper 98-3792, 34th Joint Propulsion Conference, Cleveland, OH, July 1998.
8. O. Gorshkov, AIAA paper 98-3929, 34th Joint Propulsion Conference, Cleveland, OH, July 1998.
9. V. Khayms and M. Martinez-Sanches, in *Micropropulsion for Small Spacecraft*, edited by M.M. Micci and A.D. Ketsdever (AIAA Progress in Astronautics and Aeronautics, 2000), Vol. 187, p. 45.
10. Y. Raitses and N.J. Fisch, Phys. Plasmas **8**, 2579 (2001).
11. J.P. Boeuf and L. Garrigues, J. Appl. Phys. **84**, 3541 (1998).
12. A. Smirnov, Y. Raitses, and N.J. Fisch, IEPC paper 01-038, 27<sup>th</sup> International Electric propulsion Conference, Pasadena, CA, October 2001.
13. E.A. Cubbin, J.K. Ziemer, E.Y. Choueiri, and R.G. Jahn, Rev. Sci. Instrum. **68** (6), 2339 (1997).
14. Full description of the thrust stand, the calibration procedure, as well as the measurement procedure for PPTs are given in Ref. (13). In the present paper we describe the thrust stand features relevant to a steady state Hall thruster operation only.
15. L.B. King and A.D. Gallimore, AIAA paper 98-3641, 34th Joint Propulsion Conference, Cleveland, OH, July 1998.
16. A. Bishaev and V. Kim, Sov. Phys. Tech. Phys **23**, 1055 (1978).
17. E.W. Bell, N. Djuric, and G.H. Dunn, Phys.Rev A **48**(6), 4286 (1993).
18. J.P. Marek, in *Optimal Space Trajectories*, Elsevier, Amsterdam, 1979, pp. 7-19, 38.